Flows about a Rotating Circular Cylinder by the Discrete-Vortex Method

Takeyoshi Kimura* and Michihisa Tsutahara†
Kobe University, Kobe, Japan

Introduction

A LIFT acting on a rotating circular cylinder in a uniform flow whose direction is perpendicular to the rotating axis is widely known as the Magnus effect. There are some experimental investigations[1,2] of the Magnus effect, but there are few analytical studies or numerical calculations.

Studies on the calculation of the flow past a stationary circular cylinder by the discrete-vortex method have been reported, and can be divided into two categories (depending on the method of generation of vortices). In the first category, the separation points are determined by experimental methods or by other methods, i.e., Sarpkaya and Schoaff,[3] where the nascent vortices are introduced near the separation points. In the second category, the entire boundary layer is approximated by finite-discrete vortices, as studied by Chorin[4] or Kuwahara,[5] where the separation points are not specifically considered. Kimura and Tsutahara[6] employed the latter method for the same problem considered here, and obtained results that qualitatively agreed with experimental results. However, the reverse Magnus effect, that is, the reverse lift acting on the cylinder when the rotating speed is not very high,[7,8] was not detected.

In this Note, computations were performed by the former method. In preliminary experiments, we observed the flow past a rotating circular cylinder by flow-visualization techniques and determined the separation points. In order to visualize the flows, dye injection and smoke generation by liquid titanium tetrachloride ($TiCl_4$) were used.[9] The details of the experiments are not described here, however, the values of the separation points are presented in Table 1. Here, Θ_{s1} and Θ_{s2} represent, respectively, the angles of the separation points on the deceleration side and those on the acceleration side measured from the foremost point of the cylinder, which does not correspond to a stagnation point. *Re* is the Reynolds number based on the diameter of the cylinder and α represents the spin parameter, the ratio of the peripheral speed of the cylinder to the uniform flow velocity. These preliminary experiments were performed only to obtain the parameters for numerical calculations. The data were inaccurate because we determined the separation points by observing the pictures of the flow pattern. Therefore, the angles of the separation points are shown at 5-deg intervals, but they are sufficient to estimate the effect of the distance of the separation points on the flow.

Procedure of Calculation

Mathematical formulations and methods for calculation of the forces are similar to those of Kuwahara[5] and Kimura and Tsutahara[6]; therefore we only have described a few parameters used in the present calculation.

Two nascent vortices are introduced for every time interval, $\Delta t = 0.12$ from points $z_a = (1+\epsilon)\exp(i\Theta_{s1})$ and $z_b = (1+\epsilon)\exp(i\Theta_{s2})$. ϵ is taken to be 0.02, and time is nondimensionalized by the uniform flow velocity and the radius of the cylinder. The strengths of the vortices are determined by the condition of the flow velocity that coincides with the peripheral velocity of the cylinder at $z = \exp(i\Theta_{s1})$ and $z = \exp(i\Theta_{s2})$. Once the strengths are determined, these vortices move with the local velocity of the fluid without changing their strengths. When any two vortices approach each other within a distance of σ, for example, we combine these two vortices into one. We increase σ as the vortices move away from the cylinder, so that the number of the vortices distant from the cylinder can be reduced. To reduce the computation time the velocity induced by the images inside the cylinder, for the vortices whose distance from the center of the cylinder is larger than 7.0, is estimated by assuming that

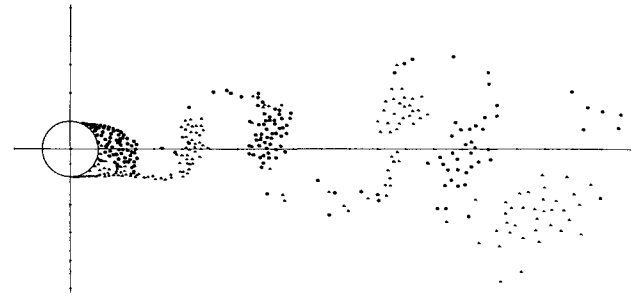

a) Distribution of vortices.

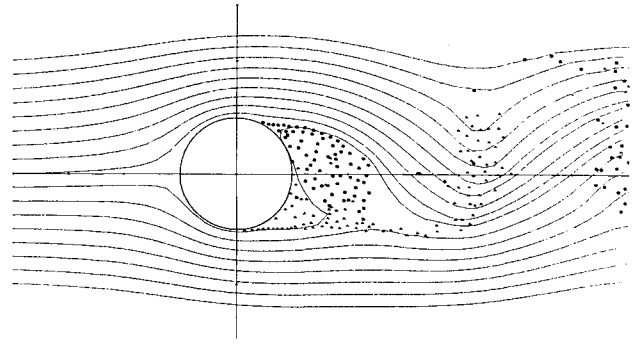

b) Streamlines at $t = 30$.

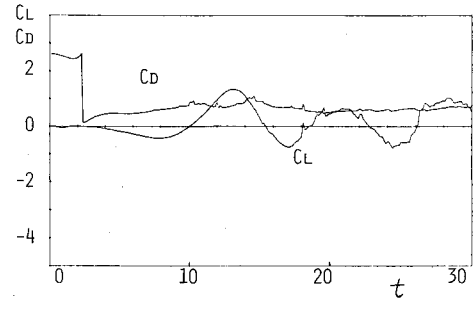

c) Time variations of lift and drag coefficients.

Fig. 1 High Reynolds number flow about rotating cylinder for $\alpha = 0.2$ (case 3): ● = negative vortices, ▲ = positive vortices.

Table 1 Observed separation points

Case	Reynolds no. ($\times 10^4$)	α	Θ_{s1}, deg	Θ_{s2}, deg
1	Subcritical	0	80	80
2	Critical	0	125	125
3	14.4	0.2	110	90
4	10.5	0.3	100	70
5	6.68	0.5	90	80
6	6.68	1.0	90	100
7	14.4	1.0	90	90
8	6.68	1.5	90	100

Received April 1, 1986; revision received July 10, 1986. Copyright © American Institute of Aeronautics and Astronautics, Inc., 1986. All rights reserved.

*Professor, Department of Mechanical Engineering.
†Associate Professor, Department of Mechanical Engineering.

all images are reduced to a single vortex at the center of the cylinder; its strength equals the sum strength of all the images.

Results

For all cases, the uniform flow and the angular velocity of the rotation of the cylinder are uniformly accelerated up to $t=2.4$; after that point they are kept constant, $U=1$ and $\omega=$ const, and the calculations are performed up to $t=30$.

The first two calculations examine the effect of the positions of the separation points for a stationary circular cylinder. Corresponding to the subcritical and the critical flows, the separation points are taken to be 80 and 125 deg, which have the same value on the accelerating and the decelerating sides. The time average of the drag coefficient for the two cases are 0.94 and 0.36, respectively, and they agree well with the widely accepted experimental data. The Strouhal number obtained from the periodic variation of the lift coefficient is 0.23 for the subcritical flow and 0.34 for the critical flow; they also agree with the experiments (see, i.e., Roshko[10]). For the case of the spin parameter $\alpha=0.2$, the distribution of the vortices, the streamlines at $t=30$, and the drag and the lift coefficients are shown in Fig. 1. The lift coefficient is periodic, but the time average of the lift coefficient has a positive value of 0.34, which means that a reverse lift acts on the cylinder. This is because the turbulent separation occurs on the acceleration side and laminar separation on the deceleration side. The separation points are $\Theta_{s1}=110$ deg and $\Theta_{s2}=90$ deg, respectively. For $\alpha=1.0$, the width of the wake region becomes narrower and the Karman-type vortices disappear. Corresponding to the disappearance, the lift coefficients do not have any predominant frequencies. This fact has been found by experiment, i.e., Diaz et al.[11] Although they did not mention any reason, by this simulation we consider it to be as follows. The vortices of opposite directions are mixed earlier in the wake as shown in Fig. 2, and the circulations in local areas become smaller. Consequently, the vortices of the same direction are neither gathered nor rolled up. The time-averaged lift coefficients are shown in Fig. 3. The solid lines in the figures are drawn from the experimental data by Swanson[1] and by Tanaka and Nagano.[2] The values for $\alpha>0.5$ obtained here are somewhat larger than Swanson's experimental results. However, they seem to agree with an extension of the results for $Re=3.71\times10^5$ by Tanaka and Nagano.[2]

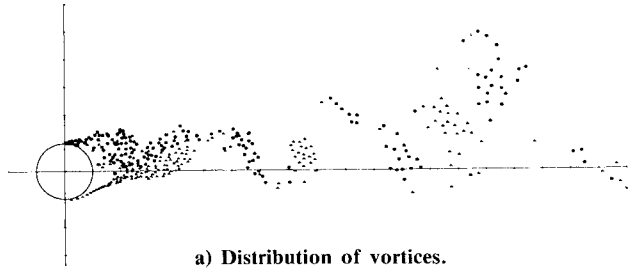

a) Distribution of vortices.

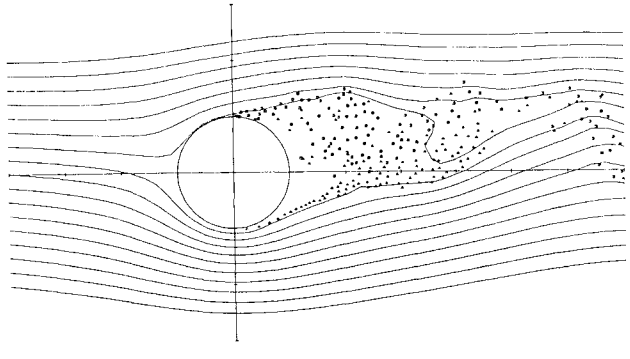

b) Streamlines at $t=30$.

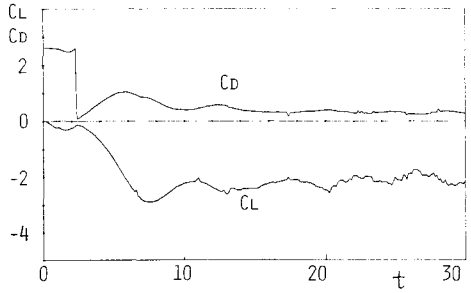

c) Time variation of lift and drag coefficients.

Fig. 2 High Reynolds number flow about rotating cylinder for $\alpha=1.0$ (case 6): ● = negative vortices, ▲ = positive vortices.

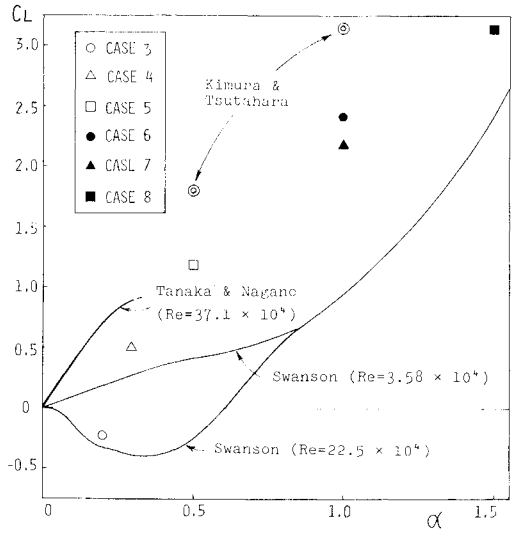

Fig. 3 Time-averaged lift coefficients. Conditions of each case are presented in Table 1; two calculated values by Kimura and Tsutahara are shown for comparison.

Conclusions

Flows past a rotating circular cylinder at high Reynolds numbers were numerically studied by the discrete-vortex method. The separation points, determined by flow visualization and nascent vortices, are introduced near these points. In the case of a stationary cylinder, the difference of the separation points in the numerical study results in the difference of drag on the cylinder between the subcritical and critical regimes. It becomes clear that the reverse Magnus effect is caused by the retreat of the separation point on the acceleration side. When the rotating speed becomes high, the nascent vortices of opposite directions are mixed faster, and the wake becomes narrower and predominant frequencies in the lift disappear.

References

[1]Swanson, W. M., "The Magnus Effect: A Summary of Investigations to Date," *Journal of Basic Engineering*, Vol. 83, Sept. 1961, pp. 461-470.

[2]Tanaka, H. and Nagano, S., "Study of Flows about a Rotating Circular Cylinder," *Journal of the Japan Society of Mechanical Engineers*, Vol. 38, 1972, pp. 1343-1352 (in Japasnese).

[3]Sarpkaya, T. and Schoaff, R. L., "Inviscid Model of Two-Dimensional Vortex Shedding by a Circular Cylinder," *AIAA Journal*, Vol. 17, Nov. 1979, pp. 1193-1200.

[4]Chorin, A. J., "Numerical Study of Slightly Viscous Flow," *Journal of Fluid Mechanics*, Vol. 57, Pt. 4, 1973, pp. 785-796.

[5]Kuwahara, K., "Study of Flow Past a Circular Cylinder by an Inviscid Model," *Journal of Physical Society of Japan,* Vol. 45, Jan. 1978, pp. 292–297.

[6]Kimura, T. and Tsutahara, M., "Flow Past a Rotating Circular Cylinder at High Reynolds Number," *Journal of Japapese Society of Aeronautical Space Sciences,* Vol. 34, April 1986, pp. 14–20.

[7]Ericsson, L. E., "Karman Vortex Shedding and the Effect of Body Motion," *AIAA Journal,* Vol. 18, Aug. 1980, pp. 935–944.

[8]Matsui, T., "Separation in a Flow past a Circular Cylinder," *Journal of Japanese Society of Aeronautical Space Sciences,* Vol. 20, Nov. 1972, pp. 18–26 (in Japanese).

[9]Freymuth, P., Bank, W., and Palmer, M., "Use of Titanium Tetrachloride for Visualization of Accelerating Flow around Airfoils," International Symposium on Flow Visualization, Ann Arbor, MI, 1983.

[10]Roshko, A., "Experiments on the Flow Past a Circular Cylinder at Very High Reynolds Number," *Journal of Fluid Mechanics,* Vol. 10, 1961, pp. 345–356.

[11]Diaz, F., Gavalda, J., Kawall, J. G., and Keffer, J. F., "Asymmetrical Wake Generated by a Spinning Circular Cylinder," *AIAA Journal,* Vol. 23, Jan. 1985, pp. 49–54.

Numerical Solutions of Viscous Transonic Flow in Turbomachinery Cascades

V. Iyer* and E. von Lavante†
Texas A&M University, College Station, Texas

Introduction

A MODIFICATION to the implicit, block-bidiagonal algorithm for solving the compressible Navier-Stokes equations is presented. The resulting method showed enhanced robustness and computational efficiency; its solution procedure requires only inversions of scalar bidiagonal matrices. In its application to several internal flow configurations, the resulting computational advantage and the importance of viscous effects in transonic cascade flow are presented.

Solution Procedure

Many of the recent studies[1-4] of cascade flow predominantly deal with the inviscid Euler equations; only isolated solution's of the full Navier-Stokes equations are presented. However, in high-solidity blade rows, there is a strong passage shock interacting with the boundary layer. The inviscid model is inadequate in such cases. The solution of the full Navier-Stokes equations is beset with difficulties in that the proximity of the shock-boundary layer region to the blade trailing edge frequently leads to strong numerical oscillations. In the present work, two numerical algorithms for solving the compressible Navier-Stokes equations are considered. They are the modified implicit bidiagonal predictor-corrector scheme by MacCormack,[5] and the approximate factorization (AF) central differenced method by Beam and Warming[6] and Steger[7]. Since it is a well-tested numerical method, the AF scheme was used for validating the modified MacCormack scheme. The initial numerical stability problems were avoided by the use of the spectral radius formulation.[8] The full implicit MacCormack scheme (FIMC) is given as follows.

Predictor step:

$$\hat{u}^{\overline{n+1}} \equiv \hat{u}^n + C_1 \cdot \Delta\hat{u}^n + C_2 \cdot \delta\hat{u}^{\overline{n+1}}$$

with

$$[I - \Delta t\Delta^+ \mid \hat{A} \mid {}^n_{ij}][I - \Delta t\Delta^+ \mid \hat{B} \mid {}^n_{ij}]C_2\delta u^{n+1}_{ij} = C_2\Delta\hat{u}^n_{ij} \tag{1}$$

Corrector step:

$$\hat{u}^{n+1} = \tfrac{1}{2}[\hat{u}^n + \hat{u}^{\overline{n+1}} + C_1\Delta\hat{u}^{\overline{n+1}} + C_2\delta\hat{u}^{n+1}]$$

with

$$[I + \Delta t\Delta^- \mid \hat{A} \mid {}^{\overline{n+1}}_{ij}][I + \Delta t\Delta^- \mid \hat{B} \mid {}^{\overline{n+1}}_{ij}]C_2\delta u^{n+1}_{ij} = C_2\Delta\hat{u}^{\overline{n+1}}_{ij} \tag{2}$$

In the above, C_1 and C_2 are constants based on the local Courant-Friedrichs-Lewy (CFL) number and $|\hat{A}|$ and $|\hat{B}|$ are 4×4 matrices derived from the Euler flux Jacobians with viscous terms added to the diagonal elements. In order to improve the efficiency of this algorithm, the $|\hat{A}|$ and $|\hat{B}|$ in the implicit step are substituted by their special radii, $\lambda_{A,SR}$ and $\lambda_{B,SR}$. For example, the spectral normal of the flux Jacobian $|\hat{A}|$ is

$$\lambda_{A,SR} = |U_\xi| + C\sqrt{\xi_x^2 + \xi_y^2} + \frac{2\nu}{\rho}\left(\xi_x^2 + \xi_y^2\right) - \frac{1}{2\Delta t} \tag{3}$$

The resulting scheme is called spectral radius implicit MacCormack (SIMC). This procedure requires only the inversion of scalar bidiagonal matrices. Temporal accuracy of the solution is lost, but the scheme becomes less susceptible to oscillations at discontinuities. As it turns out, steady state accuracy is also compromised. This is due to the fact that the residual $\delta\hat{u}$ stays at relatively high values after decreasing by three orders of magnitude, especially in viscosity dominated regions where the largest eigenvalues of $|\hat{A}|$ and $|\hat{B}|$ are not dominant.

The SIMC scheme is ideally suited as an efficient scheme to obtain approximate viscous solutions. To enhance the steady-state accuracy, the full schemes are subsequently employed for a relatively small number of iterations. In the present analysis, several cases of internal flow geometries were studied. In each case, the SIMC was used as a preprocessor. Comparisons of convergence times are presented and are given in Ref. 9. Some comparisons with the inviscid results (wherever available) are also given and have demonstrated the importance of including the viscous terms in transonic cascade analysis.

Results

Initially, simpler geometries were selected to validate the codes and compare computation times, convergence rates, and quality of results. The results for the case of a supersonic nozzle and a diffusor with oblique shock have been previously reported.[8] Results of further flow predictions done for complex geometries are presented here (additional details are found in Ref. 10).

The flow past a wedge enclosed in a two-dimensional tunnel section is an internal flow configuration involving shocks and expansion waves and their interaction with the boundary layer. The geometry corresponds to the experimental arrangement reported in Ref. 11, which also contains the results of computations using the Euler equations. The wedge semi-angle is 9 deg, and the inflow Mach number is 1.45. The flow undergoes an oblique shock at the wedge and an expansion at the tunnel wall. Further downstream, the tunnel wall produces

Presented as Paper 85-0007 at the AIAA 23rd Aerospace Sciences Meeting, Reno, NV, Jan. 14–17, 1985; received Oct. 15, 1985; revision received April 23, 1986. Copyright © American Institute of Aeronautics and Astronautics, Inc., 1985. All rights reserved.

*Graduate Research Assistant; presently Research Engineer, Vigyan Research Associates Inc., Hampton, VA. Member AIAA.

†Assistant Professor, Aerospace Engineering Department; presently Associate Professor, Old Dominion University, Norfolk, VA. Member AIAA.